Earthquake Engineering, Tenth World Conference © 1992 Balkema, Rotterdam. ISBN 90 5410 060 5

Finite element analysis of shear resistance of masonry wall panels with and without confining frames

P.B. Shing, H.R. Lotfi, A. Barzegarmehrabi & J. Brunner
University of Colorado, Boulder, Colo., USA

ABSTRACT: Finite element models based on the smeared- and discrete-crack approaches have been developed to evaluate the shear resistance of masonry walls and masonry infilled reinforced concrete frames. The capabilities of these models in capturing the strength and various failure mechanisms of such structures are examined, and crucial modeling considerations are identified. It is shown in this study that the above models can be used to reproduce experimental results with a high degree of accuracy. However, it is observed that numerical results are highly dependent on the finite element idealization, and that the inelastic behavior of an infilled frame is very sensitive to the shear strength of the mortar joints in the masonry infill.

1 INTRODUCTION

Masonry panels exist as shear walls in masonry structures or infill walls for reinforced concrete frames. While the former is generally designed as major shear resisting members for modern reinforced masonry structures, the latter is often considered as non-structural components, such as partition walls. However, both laboratory studies and damage observations from past earthquakes have indicated that the interaction of masonry panels with reinforced concrete frames has a profound influence on the performance of an infilled structure. In any respect, the shear resisting mechanisms of masonry walls with and without confining frames are not well understood. In this paper, finite element models based on the smeared- and discrete-crack approaches are presented to evaluate the behavior of such structures.

The analysis of masonry structures has been based very much on the modeling techniques developed in concrete mechanics and rock mechanics. Nevertheless, the behavior of masonry is far more complex than that of concrete or rocks. While concrete does not have the inherent planes of weakness introduced by mortar joints, the behavior of rock mass is often dominated by rock joints. On the other hand, in masonry, it is important to consider the failure of the mortar joints as well as masonry units. In this respect, various modeling approaches have been proposed and customized for masonry structures. One approach is to homogenize a masonry assembly and represent the average elastic properties by means of an equivalent homogeneous model, in which the nonlinear behavior of masonry can be modeled by the viscoplasticity theory with the viscoplastic strain of each constituent material evaluated separately using an appropriate constitutive model (Middleton et al. 1991). While the aforementioned approach is computationally efficient in that the finite element discretization does not have to conform to the actual locations of the mortar joints, it cannot adequately model refined crack patterns in masonry assemblies. Hence, one alternative is to use the smeared-crack approach, which has been widely used to analyze the fracture behavior of concrete structures. However, in this approach, it is difficult to incorporate the influence of mortar joints in the fracture behavior of masonry. Hence, it has been predominantly used for modern masonry that consists of hollow units and solid grout, where the influence of mortar joints is relatively insignificant (Ewing et al. 1988; Shing and Lotfi 1991). The most refined approach is to model the masonry units and mortar joints separately with continuum elements, which can be linked by interface elements to allow for the shear-dominated interface mechanisms (Anand and Rahman 1990). While the modeling of mortar joints with continuum elements is important for detailed stress analysis (Rots 1991), it requires very refined meshes and is, therefore, not suitable for analyzing large structural components. In this respect, a more efficient alternative is to model mortar joints with interface elements alone (Page 1978; Rots 1991).

In view of the above considerations, two types of element models have been developed in this study. One is a smeared-crack model that can be used to simulate the distributed tension and compression failure of masonry units and concrete members, and

the other is an interface model that can be used to simulate discrete crack opening in masonry units and mortar joints, as well as the interface behavior between infill panels and the bounding frames. Both the model formulations and numerical results are presented in this paper. Using these models, the smeared- and discrete-crack approaches are examined and compared, and the shear strengths and failure mechanisms of masonry wall panels with and without confining frames are analyzed. The numerical results are compared with experimental data, and crucial modeling considerations are identified.

2 CONSTITUTIVE MODELS AND FINITE ELEMENT FORMULATIONS

2.1 Smeared-crack model

The smeared-crack approach has been widely used to model diffuse cracks in concrete structures and is a convenient way to model the tensile fracture of masonry units. It is computationally efficient in that it does not require a large number of degrees of freedom to model crack propagation. In this study, an elastic-plastic plane-stress model based on the von Mises yield criterion and associated flow rule, combined with a Rankine-type tension cutoff, is adopted. The former is used to simulate the compressive fracture of concrete and masonry. The failure criteria are shown in Fig. 1, in the space of principal stresses, σ_1 and σ_2. Tensile cracking occurs when the tension-cutoff surface is reached. This transforms the material behavior from elastic-plastic to nonlinear orthotropic with the axes of orthotropy parallel and perpendicular to the crack. Both fixed and rotating crack formulations are implemented. Appropriate post-peak softening rules are incorporated for tension and compression. The detail of the model can be found elsewhere (Shing and Lotfi 1991).

2.2 Reinforcing steel

Reinforcing steel is modeled as an elastic-hardening plastic material. It is formulated in two ways. One is a discrete bar element and the other is a smeared overlay on top of a smeared-crack element, with the strain compatibility between the steel and masonry assumed in both cases. In either case, only the uniaxial stress-strain relation in each reinforcing direction is considered. Dowel action is not incorporated in the model, but can be approximately accounted for by means of the shear retention feature in the crack model.

2.3 Interface model

Various plasticity laws have been proposed for interface behavior. Plesha (1987) has adopted a yield surface based on Coulomb friction for modeling the slippage of rock joints. This model, however, does not account for the tensile strength of an interface. Stankowski (1990) has incorporated fracture energy concepts into an elastic-softening plastic model for simulating the micro-fracture process of concrete. Prat et al. (1991) has proposed a similar model based on a hyperbolic yield surface. In all these models, nonassociated flow rules and different work softening laws have been adopted. The interface model used here is similar in concept to the above models, but with a yield criterion, plastic potential, and softening laws that are able to capture a wide range of fracture behavior of concrete as well as masonry mortar joints. The detail of the model has been documented by Lotfi and Shing (1992), and its main features are briefly summarized in the following.

Based on the plasticity theory, the relative displacements $\underline{\alpha}$ between the two contact surfaces of an interface can be decomposed into an elastic component $\underline{\alpha}^e$ and a plastic component $\underline{\alpha}^p$ as

$$\underline{\alpha} = \underline{\alpha}^e + \underline{\alpha}^p \tag{1}$$

in which $\underline{\alpha} = \{\alpha_n \quad \alpha_t\}^T$, where α_n and α_t are the relative normal and tangential displacements, respectively. The elastic displacements are related to the interface stresses by the following equation:

$$\dot{\underline{\alpha}}^e = \underline{D}^{-1}\dot{\underline{\sigma}} \tag{2}$$

in which $\underline{\sigma} = \{\sigma \quad \tau\}^T$, where σ and τ are the normal and tangential interface stresses, the superposed dot represents differentiation with respect to time, and $\underline{D} = \text{Diag}[k_{nn} \quad k_{tt}]$, a diagonal matrix of elastic constants.

The failure surface of the interface model adopted is represented by a hyperbolic curve in the $\sigma-\tau$ space, as shown in Fig. 2, and is expressed in the following form:

$$F(\underline{\sigma}, \underline{q}) = \tau^2 - \mu^2(\sigma - s)^2 - 2r(\sigma - s) = 0 \tag{3}$$

in which $\underline{q} = \{\mu \quad s \quad r\}^T$, representing the internal variables of the material, where μ is the slope of the asymptotes of the yield surface, s is the tensile resistance of the interface, and $-r$ is the radius of curvature at the vertex of the hyperbola. The cohesion c can be expressed as $\sqrt{\mu^2 s^2 - 2rs}$ (see Fig. 2). The evolution of the internal variables $\underline{q}$ is governed by the following work softening rules:

$$s = s_0\left(1 - \frac{\kappa_1}{G_f^I} - \frac{\kappa_2}{G_f^{II}}\right) \tag{4}$$

$$r = r_r + (r_0 - r_r)e^{-\beta\kappa_3} \tag{5}$$

$$\mu = \mu_r + (\mu_0 - \mu_r)e^{-\alpha\kappa_3} \tag{6}$$

in which the subscripts 0 and r represent the initial and residual values of the internal variables (see Fig. 2), α and β are material parameters that govern the rate of deterioration of the frictional resistance in the interface, and G_f^I and G_f^{II} can be considered as the fracture energies related to mode I and mode II fracture. When the curvature r is zero, the failure surface is reduced to the Mohr-Coulomb criterion. The work softening parameters $\underline{\kappa} = \{\kappa_1 \quad \kappa_2 \quad \kappa_3\}^T$ are defined as follows.

$$\dot{\kappa}_1 = <\sigma>\dot{\alpha}_n^p \tag{7}$$

$$\dot{\kappa}_2 = (\tau - \tau_{r1})\dot{\alpha}_t^p \tag{8}$$

$$\dot{\kappa}_3 = (\tau_{r1} - \tau_{r2})\dot{\alpha}_t^p \tag{9}$$

in which $<\cdot>$ is the Macauley bracket, and

$$\tau_{r1} = \sqrt{\mu^2\sigma^2 + 2r\sigma} \tag{10}$$

$$\tau_{r2} = \sqrt{\mu_r^2\sigma^2 + 2r_r\sigma} \tag{11}$$

The above work softening laws utilizing the fracture energy concept are an enhancement of the version proposed by Stankowski (1990). The plastic displacement is governed by a nonassociated flow rule:

$$\underline{\dot{\alpha}}^p = \dot{\lambda}\frac{\partial Q}{\partial \underline{\sigma}} \tag{12}$$

where the plastic potential is given by

$$Q(\underline{\sigma}, \underline{q}) = \eta\tau^2 - (r - r_r)(\sigma - s) \tag{13}$$

in which η is a material parameter that governs shear dilatancy. The above expression takes into account the phenomenon that the shear dilatancy decreases as the interface compressive stress increases or when the contact surfaces are smoothened by frictional work. The loading and unloading satisfy the Kuhn-Tucker conditions:

$$F \le 0 \quad , \quad \dot{\lambda} \ge 0 \quad , \quad F\dot{\lambda} = 0 \tag{14}$$

The above formulations lead to the following elastoplastic material law:

$$\dot{\underline{\sigma}} = \underline{D}^{ep}\dot{\underline{\alpha}} \tag{15a}$$

where

$$\underline{D}^{ep} = \underline{D} - \frac{\underline{D}\,\underline{m}\,\underline{n}^T\underline{D}}{\underline{n}^T\underline{D}\,\underline{m} - \underline{p}^T\underline{t}} \tag{15b}$$

$$\underline{n} = \frac{\partial F}{\partial \underline{\sigma}} \quad , \quad \underline{m} = \frac{\partial Q}{\partial \underline{\sigma}} \quad , \quad \underline{p} = \frac{\partial F}{\partial \underline{q}} \quad , \quad \underline{t} = \frac{\partial q}{\partial \underline{\kappa}}\underline{H}\underline{m} \tag{15c}$$

$$\underline{H} = \begin{bmatrix} <\sigma> & 0 \\ 0 & \tau - \tau_{r1} \\ 0 & \tau_{r1} - \tau_{r2} \end{bmatrix} \tag{15d}$$

In computation, for a given relative displacement increment $\Delta\underline{\alpha}$, the stress increment $\Delta\underline{\sigma}$ is evaluated by a generalized mid-point rule (Ortiz and Popov 1985). The above model is implemented in 4- and 6-noded isoparametric interface elements.

3 MASONRY SHEAR WALLS

The analysis of a fully grouted reinforced masonry concrete block wall is first presented. The wall was tested as part of the U.S.-Japan Coordinated Program for Masonry Building Research (Shing et al. 1989). As shown in Fig. 3, the wall was subject to a constant axial compressive stress of 100-psi (0.689 MPa) and lateral cyclic load reversals at the top. The reinforcing bars were uniformly spaced in both directions, with five No. 7 bars in the vertical direction and five No. 3 bars in the horizontal direction. The wall exhibited a brittle shear failure with distinct diagonal cracks. Four-node quadrilateral smeared-crack elements with co-axial rotating cracks and an overlay of steel reinforcement have been used in the analyses. The first analysis has been conducted with purely smeared-crack elements, and the second with interface elements along one of the wall diagonals in additional to the smeared-crack elements. The lateral displacement has been varied monotonically in both analyses.

The deformed mesh with interface elements is shown in Fig. 4, and the crack pattern is shown in Fig. 5. The numerical results are compared to the experimental load-displacement envelope in Fig. 6. It can be observed that the result without interface elements significantly overestimates the shear strength of the wall. This problem of smeared-crack models is caused by the continuum formulation of the crack elements, as explained by Shing and Lotfi (1991). The model with interface elements has a shear strength close to the experimental result, but appears to be more ductile than the test specimen. This is partly due to the different load histories applied in the analysis and in the test.

An unreinforced masonry wall with window and door openings has also been analyzed to demonstrate the possible failure mechanism of such a structure. The brick units have been modeled with linearly elastic quadrilateral elements, while the mortar joints have been modeled with interface elements. The mortar joints are assumed to have a tensile strength of 50 psi (0.344 MPa), and a shear strength of 50 psi (0.344 MPa) under a compressive stress of 5 psi (0.034 MPa). The wall has been subjected to base acceleration in the form of a single-cycle sine pulse that has a period of 0.3 sec. and an amplitude of 0.8g. The masonry is assumed to have a weight density of 150 pcf (23.6 kN/m^3) and the wall also carries a roof load of 700 lb/ft. (10.2 kN/m). The total base shear developed is shown in Fig. 7 and the deformed mesh is shown in Fig. 8.

4 MASONRY INFILLED R/C FRAMES

A reinforced concrete frame infilled with brick masonry, which was tested by Fiorato et al. (1970), has been analyzed. The frame was subjected to a monotonic in-plane lateral load applied at the top. The concrete frame and masonry infill have been modeled with smeared-crack elements. The flexural reinforcement in the frame has been modeled with discrete bar elements, while the shear reinforcement modeled with an overlay of smeared steel. Three analyses have been conducted: (1) without any interface elements; (2) interface elements used to model the frame-panel interfaces only; and (3) interface elements used to model the mortar joints as well as the frame-panel interfaces. It should be noted for case (3) that to allow for a relatively coarse mesh, the locations of the mortar joints are not exactly represented. Furthermore, interface elements are inserted at critical locations in the columns at approximately 45-degree angles to allow shear failure. The deformed mesh is shown in Fig. 9, the crack pattern is shown in Fig. 10, and the lateral load-vs.-lateral displacement curves are shown in Fig. 11. It can be observed that the interface elements are essential for capturing the separation of the frame-panel interfaces and the horizontal sliding failure of the mortar joints. Furthermore, the numerical results are highly sensitive to the shear strength specified for the mortar joints.

5 CONCLUSIONS

This study indicates that the failure of reinforced and unreinforced masonry wall panels, with and without confining frames, can be adequately modeled with a combination of smeared-crack and interface elements. However, the smeared-crack approach alone is not able to capture the brittle shear failure of a wall panel and to account for the influence of mortar joints. The use of interface elements in a discrete crack approach can improve numerical results, but its usage requires the knowledge of the location and orientation of the critical crack as a *priori*. The behavior of an infilled frame can be highly sensitive to the shear strength of the mortar joints in the masonry infill. Such information appears to be important in order to have an accurate assessment of the seismic resistance of infilled structures.

ACKNOWLEDGMENTS

The study presented in this paper is supported by the National Science Foundation under Grant Nos. BCS-8658100 and MSM-8914008. Partial support of the Western States Clay Products Association is also appreciated. However, opinions expressed in this paper are those of the writers, and do not necessarily represent those of the sponsors.

REFERENCES

Anand, A.C. and Rahman, M.A. 1990. Interface behavior in concrete block mortar joints - a comparison of analytical and experimental results. *Proc. of Fifth North American Masonry Conf.*, II, University of Illinois, Urbana-Champaign, IL: 475-486.

Ewing, R.D., El-Mustapha, A.M., and Kariotis, J.C. 1988. A finite element computer program for the nonlinear static analysis of reinforced masonry walls. *Proc. of Eighth Int. Brick/Block Masonry Conf.*, Dublin, Ireland.

Fiorato, A.E., Sozen, M.A., and Gamble, W.L. 1970. An investigation of the interaction of reinforced concrete frames with masonry filler walls. *Struct. Research Series No. 370*, University of Illinois, Urbana-Champaign, IL.

Lotfi, H.R. and Shing, P.B. 1992. An interface model applied to masonry structures. (*in preparation*)

Middleton, J., Pande, G.N., Liang, J.X., and Kralj, B. 1991. Some recent advances in computer methods in structural masonry. *Computer Methods in Structural Masonry*, J. Middleton and G.N. Pande, eds., Books and Journals International, Swansea, UK: 1-21.

Ortiz, M. and Popov, E.P. 1985. Accuracy and stability of integration algorithms for elasto-plastic constitutive relations. *Int. J. of Num. Meth. Eng.*, Vol. 21: 1561-1575.

Page, A.W. 1978. Finite element model for masonry. *J. of Struct. Div.*, ASCE, 104(8): 1267-1285.

Plesha, M.E. 1987. Constitutive models for rock discontinuities with dilatancy and surface degradation. *Int. J. of Num. Anal. Meth. Geomech.*, 11: 345-362.

Prat, P.C., Carol, I., and Gettu, R. 1991. Numerical analysis of mixed-mode fracture of quasi-brittle materials using a multicrack constitutive model. *Proc. of Int. Conf. on Mixed-Mode Fracture and Fatigue*, Vienna, Austria.

Rots, J.G. 1991. Computer simulation of masonry fracture: continuum and discontinuum models. *Computer Methods in Structural Masonry*, J. Middleton and G.N. Pande, eds., Books and Journals International, Swansea, UK: 93-103.

Shing, P.B., Noland, J.L., Klamerus, E., and Spaeh, H. 1989. Inelastic behavior of concrete masonry shear walls. *J. of Struct. Engrg.*, ASCE, 115(9): 2204-2225.

Shing, P.B. and Lotfi, H.R. 1991. Experimental and finite element analyses of single-story reinforced masonry shear walls. *Computer Methods in Structural Masonry*, J. Middleton and G.N. Pande, eds., Books and Journals International, Swansea, UK: 74-83.

Stankowski, T. 1990. Numerical simulation of progressive failure in particle composites. *Ph.D. Thesis*, University of Colorado, Boulder, CO.

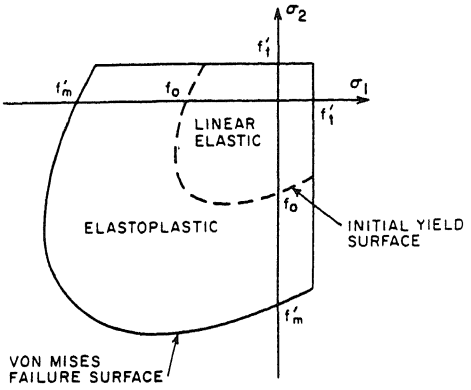

Figure 1. Yield and failure criteria for smeared-crack model

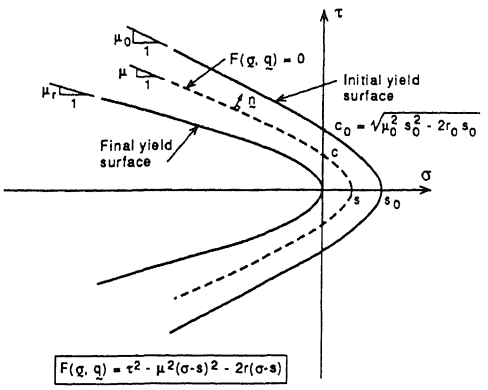

Figure 2. Failure surface of interface model

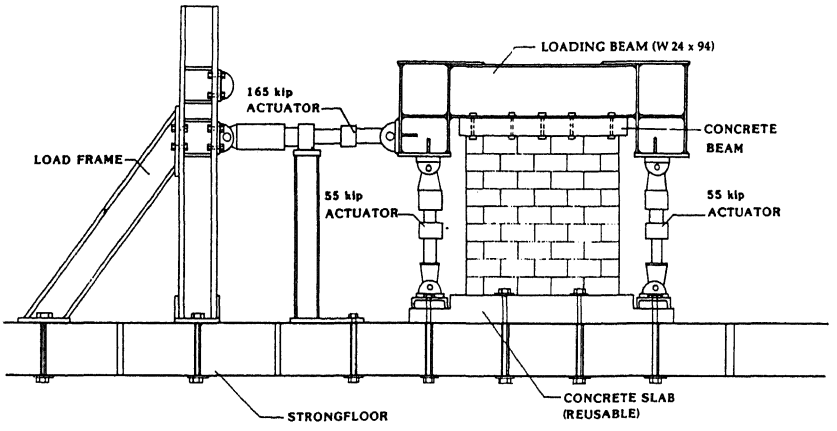

Figure 3. Test of reinforced masonry wall

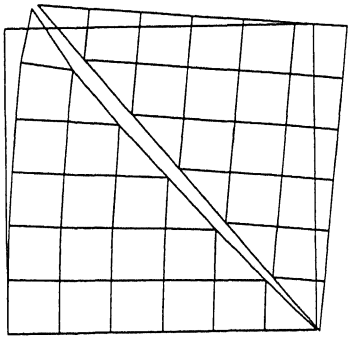

Figure 4. Deformed mesh of reinforced masonry wall

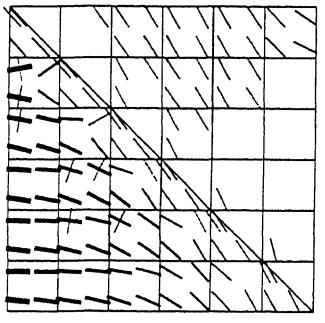

Figure 5. Crack pattern of reinforced masonry wall

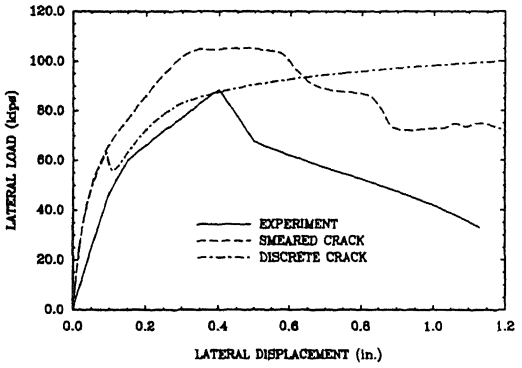

Figure 6. Load vs displacement curve of reinforced masonry wall

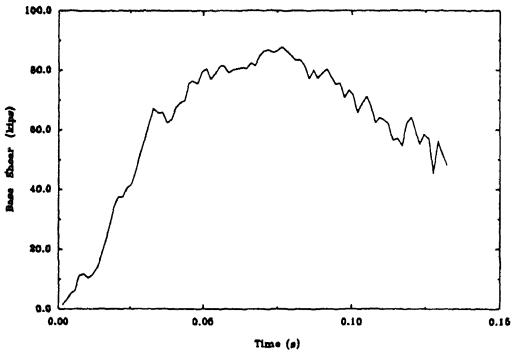

Figure 7. Base shear of unreinforced brick wall

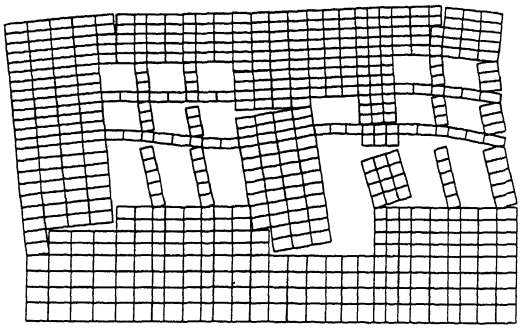

Figure 8. Deformed mesh of unreinforced brick wall

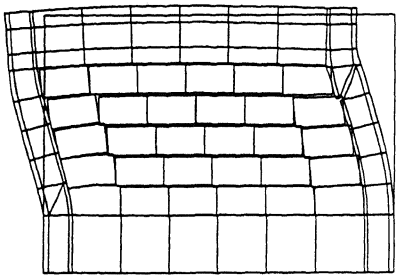

Figure 9. Deformed mesh of infilled frame

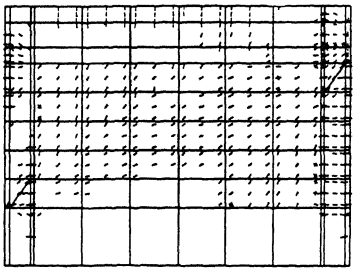

Figure 10. Crack pattern of infilled frame

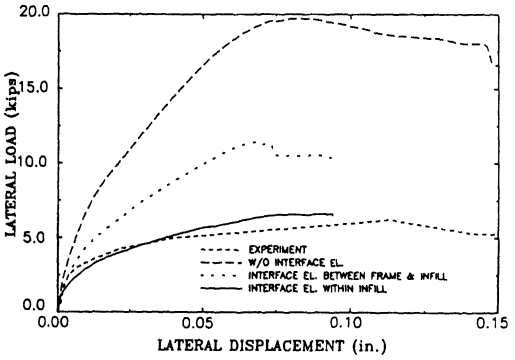

Figure 11. Load vs displacement curve of infilled frame